The influence of commercial Ionomers and Membranes on a PGM-free catalyst in the Alkaline Oxygen Reduction

Simon Kellner [a], Ziyang Liu [a], Francesco D'Acierno [a], Angus Pedersen [a], Jesús Barrio [a], Sandrine E. M. Heutz [b], Ifan E. L. Stephens [b], Silvia Favero [a], Maria-Magdalena Titirici [a,*]*

[a] Department of Chemical Engineering, Imperial College London, London SW7 2AZ, United Kingdom

[b] Department of Materials, Royal School of Mines, Imperial College London, London SW7 2AZ, United Kingdom

KEYWORDS alkaline exchange ionomer, alkaline exchange membrane, PGM-free catalysts, Fe-N-C catalyst, gas diffusion electrode, oxygen reduction reaction, fuel cell

ABSTRACT Hitherto, research into alkaline exchange membrane fuel cells (AEMFCs) lacks a commercial benchmark anionomer and membrane, analogue to Nafion™ in proton-exchange membrane fuel cells (PEMFCs). Three commercial alkaline exchange ionomers (AEI) are scrutinized for that role in combination with a commercial platinum-group-metal free (PGM-free) Fe-N-C (Pajarito Powder) catalyst for the cathode. Initial rotating disc electrode (RDE) benchmarking of the Fe-N-C catalyst's oxygen reduction reaction (ORR) activity using Nafion™

in alkaline electrolyte seems to neglect the restricted oxygen diffusion in the AEIs, and is recommended to be complemented by measurements with the same AEI as used in the AEMFC testing. Evaluation of the catalyst layer in a Gas-Diffusion-Electrode (GDE) setup offers a way to assess the performance in realistic operating conditions, without the additional complications of device-level water management. Blending of a porous Fe-N-C catalyst with different types of AEI yields catalyst layers with different pore size distributions. The catalyst layer with Piperion® retains the highest proportion of the original BET surface area of the Fe-N-C catalyst. The water adsorption capacity is also influenced by the AEI, with Fumion FAA-3® and Piperion® having equal high capabilities surpassing Sustainion®. Finally, the choice of the membrane influences the ORR performance as well, particularly the low hydroxide conductivity of Fumion FAA-3® at the room temperature experiments mitigates the ORR performance irrespective of the AEI in the catalyst layer. The best overall performance at high current densities is shown by Piperion® AEI matched with Sustainion® X37-50 AEM.

1. Introduction

For the last sixty years, research in proton-exchange-membrane fuel cells (PEMFCs) has benefit from Nafion™ membranes, which have been developed by Walther Grot and patented by DuPont.[1] In 2023, the European Chemicals Agency (ECHA) proposed a ban for per- and polyfluoroalkyl substances, including Nafion™, whose chemical structure is based on a perfluorinated polymer backbone functionalized with sulfonic acid groups.[2] This potential restriction on Nafion™ could benefit hydrocarbon-based anion conducting polyelectrolytes, which are cheaper and safer to produce.[3] The progress in anion conducting polyelectrolyte development over the past twenty years has accelerated research on alkaline exchange membrane fuel cells (AEMFCs).[4] In

AEMFCs, PtRu/C is usually used as the anode benchmark catalyst, while Pt/C is used at the cathode. Recently, PGM-based AEMFCs achieved a breakthrough into peak power densities > 2 W/cm^2 (Table S1).[5,6,7] As the ORR is more favourable with faster electrochemical kinetics in alkaline, the catalyst loading at the cathode can be reduced. Alternatively, the cathode PGM-catalyst can be substituted by a PGM-free catalyst such as Fe-N-C catalyst materials, which are among the best performing PGM-free catalysts in alkaline environment.[8,9,10,11,12] The only commercial catalyst among the AEMFC cathodes exceeding the peak power density level of 1 W/cm^2 is Fe-N-C Pajarito Powder (Table S2).[13,14,15]

The critical component in AEMFCs is the anion conducting polyelectrolyte applied as ionomer (AEI) in the catalyst layers and as membrane (AEM) between anode and cathode.[16] While the requirement on the anion conducting polyelectrolyte differs depending on the application as either AEI or AEM, both need sufficient ion conductivity for hydroxide ion (OH^-) transport. AEMs are positioned between anode and cathode to block hydrogen and oxygen cross-over, whereas AEIs are a component of anode and cathode catalyst layers acting as binder and supply anions to the triple-phase boundary. Therefore, AEMs require good gas barrier properties[17] and limited water contents to minimize membrane swelling, while AEIs need high water permeability, fast oxygen transport, and minimal blocking of electrocatalysts active sites accessibility. Ideally, the development of AEIs and AEMs should take place separately to design the properties of the material for the specific function.[18] The reader is referred to recent reviews covering the materials development for AEIs[19] and for AEMs[20]. The rapid development led to scale up and commercialization of anion conducting polyelectrolyte technologies, such as those offered by FUMATECH BWT GmbH, Versogen Inc. and Dioxide Materials Inc.

Gas-Diffusion-Electrodes (GDEs) offer an intermediate opportunity between rotating disk electrode measurements and membrane electrode assembly (MEA) to focus on the characterization of an individual application-relevant catalyst layer.[21] The utilization of the catalyst can be maximized by tailoring the ionomer to catalyst ratio, the efficiency of water and O_2 mass transport can be enhanced by fine-tuning the microstructure via the choice of solvents in the ink[22], and the optimal total loading of catalyst can be determined. The door towards alkaline studies in a GDE setup was opened with a study of commercial Aemion™ ionomer with Pajarito Powder's Fe-N-C catalyst with focus on the activation time of the catalyst layer and catalyst durability.[23] We recently reported the performances of a biomass-derived Fe-N-C and Pajarito Powder Fe-N-C at alkaline pH in the small GDE half-cell[24] employing Sustainion® XA-9 ionomer and Sustainion's X37-50® membrane.[25] Following up on our previous results, in this work we present an extensive study on cathode catalyst layers based on Fe-N-C from Pajarito Powder and the three AEIs including Fumion® FAA-3 (abbrev.: Fumion AEI), PiperION® (abbrev.: Piperion AEI), and Sustainion® XA-9 (abbrev.: Sustainion AEI), which differ in their molecular structures (Figure S1). In contrast to the Aemion™ study[23], in the GDE employed in this work the catalyst layer is separated by a membrane from the liquid electrolyte compartment to prevent flooding of the catalyst layer and this configuration enables to assess the effect of cross-combining the selected ionomer with the membrane equivalents of Fumasep® FA-3-50 (FumaTech) (abbrev.: Fumasep AEM), PAP-TP-85® (Piperion AEM) (abbrev.: Piperion AEM) and X37-50® (Sustainion) (abbrev.: Sustainion AEM) (Scheme 1). The effect of the ionomer interaction with Fe-N-C catalyst was characterized ex-situ in a rotating disc electrode (RDE) study combined with small angle X-ray scattering (SAXS) study. The ORR performance of the sprayed catalyst layers was assessed in a gas-diffusion-electrode (GDE) cell. Correlations between the ORR performance and (i) catalyst

morhology, as observed in SEM imaging and porosimetry , (ii) water uptake, and (iii) gas diffusion properties by means of O_2 limiting current measurements were established. In addition, the choice of the AEM with its intrinsic hydroxide conductivity impacted the measured ORR performance.

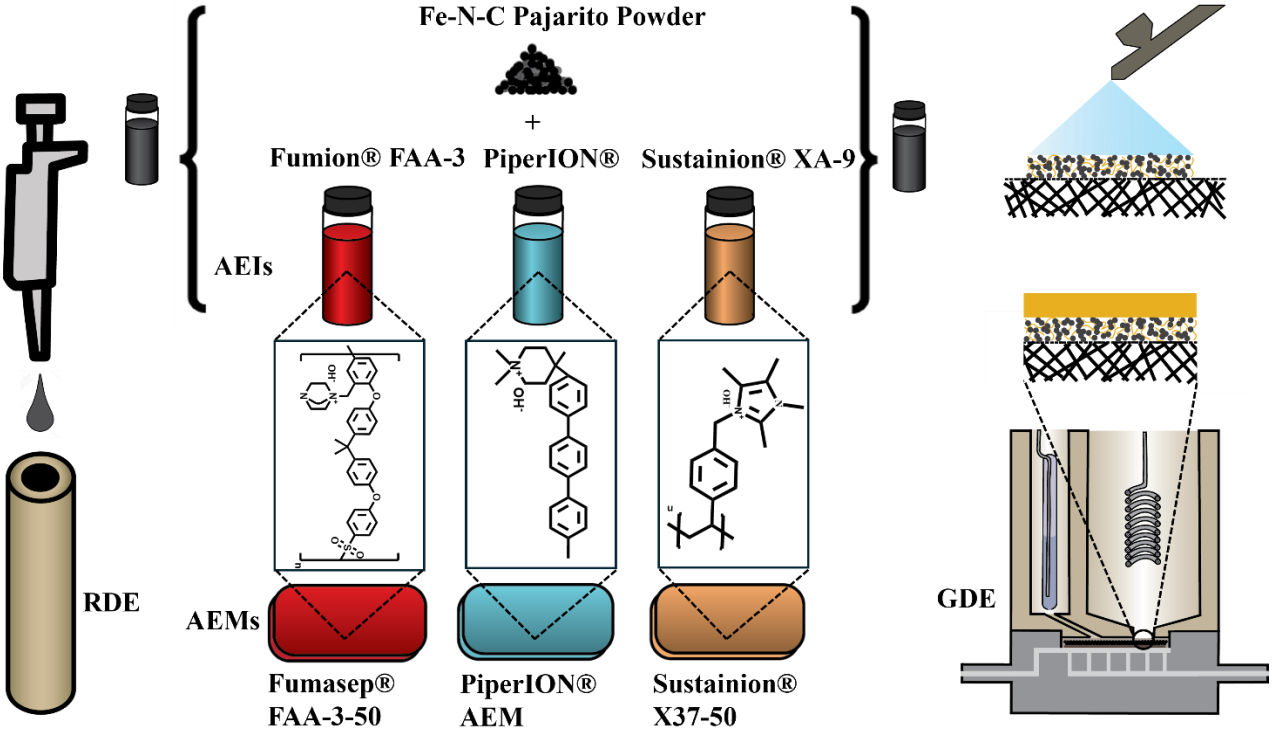

Scheme 1. Inks based on commercial Fe-N-C Pajarito Powder and one of three types of commercial AEI respectively is either drop casted on the RDE or sprayed onto gas-diffusion layer. The gas-diffusion-electrode is attached to a commercial AEM and tested in a gas-diffusion-electrode half-cell (Molecular structures are also displayed in Figure S1.).

2. Results and Discussion

2.1. Rotating Disc Electrode (RDE) study of AEIs and SAXS measurement of RDE inks

The RDE is the most conventional method to benchmark the catalytic activity in the kinetic region. Routinely, Fe-N-C catalyst are dispersed in an ink composed of ionomer and solvents and that ink is drop casted on glassy carbon electrode with a loading commonly in the range of 200µg/cm^2 - 800µg/cm^2. Recently, the analysis of RDE studies of Fe-N-C catalysts observed that the metric of half-wave potential increases as the RDE catalyst loading is increased. It is concluded that the mass activity is the better metric for intrinsic activity than the half-wave potential.[26] Lower loadings are recommended, as the high loadings may diminish the mass activity due to transport losses and lower accessibility to active sites. Therefore, a catalyst loading of 200µg/cm^2 is chosen in this work. It is important to highlight that RDE studies of ionomers can provide limited information, masking the role of the ionomer in water management, its performance at low humidity and even its anion-conductivity, since in a liquid environment this property is not critical. Nevertheless, RDE can give insights into specific properties on the ionomer, including those that affect catalyst layer morphology and kinetics. Furthermore, thanks to its simplicity, RDE is the most commonly employed technique and therefore it is of great interest to assess the capability and limitations of this technique in predicting the performance of ionomers in real devices. Even though Nafion‘s molecular structure contains sulfonic acid groups for proton transport in acidic electrolyte, Nafion ionomer is used as ionomer in the majority of RDE studies in alkaline electrolyte.[27,28] The effect of the presence of different commercial ionomers Nafion, Fumion, Piperion and Sustainion on the ORR performance of a commercially available Fe-N-C catalyst (Pajarito Powder) is compared (Figure 1 a)). Even though the catalyst nature, loading and ink composition is kept constant for all ionomers, the cyclic voltammograms in oxygen saturated

0.1 M KOH are quite different. In the entire potential range, the combination with Nafion has the best activity followed by Fumion and Sustainion, with very similar performance. The combination of the Fe-N-C catalyst with Piperion shows the worst kinetic performance. It has already been reported that the use of Fumion instead of Nafion in RDE leads to a lower kinetic current density with Fe-N-C and metal-free catalysts.[29,30] The mass activities at 0.85 V rank from the highest with Nafion (30.35 A/g), to Fumion (10.90 A/g), to Sustainion (9.65 A/g) to the lowest with Piperion (2.05 A/g). A same trend can be found for the limiting current density at 0.2 V, the highest limiting current was found with Nafion (5.18 mA/cm^2) followed by Fumion (3.78 mA/cm^2), Sustainion (3.68 mA/cm^2) and Piperion (2.98 mA/cm^2). Theoretically, the diffusion limiting currents at around the calculated value of 5.97 mA/cm^2 at 1600 rpm on a 5 mm diameter working electrode in 0.1 M KOH are expected.[31] Obviously, the AEIs are blocking the transport of oxygen to the catalysts' active site, whereas in the case of Nafion the oxygen transport is not restricted.

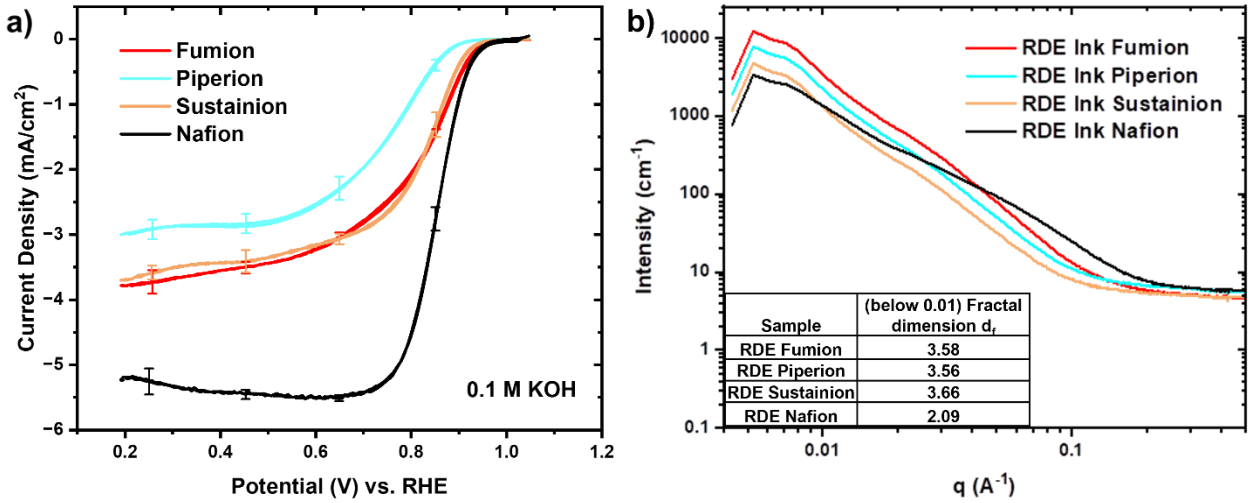

Figure 1. a) Cyclic voltammetry (CV) of Fe-N-C Pajarito Powder catalyst with respective ionomer Fumion, Piperion, Sustainion and Nafion (33% Ionomer / 66% Catalyst) starts at a potential of 0.20 V_{RHE} with a 10 mV/s scan rate in anodic scan direction in oxygen-saturated 0.1 M KOH at 1600 rpm. The catalyst loading of 200 $\mu g_{Fe\text{-}N\text{-}C}/cm^2$ is measured on a glassy carbon electrode (Ø = 5 mm) (WE) in a cell containing a glassy carbon rod (CE) and Hg/HgO (RE). The applied voltage is corrected for iR drop determined by EIS post measurement. The average of a set of three independent measurements for each sample is plotted with error bars. b) SAXS scattering curves of catalyst inks for RDE.

The RDE inks are investigated in SAXS to gain insights into the agglomerates of ionomer and catalyst in the ink. The scattered intensity (I(q)) is plotted versus the scattering vector (q) for the four different inks (Figure 1. b)). The power-law scaling exponent of the intensity at low q (< 0.01Å^{-1}) in I(q) ~ q^{-d_f} is called fractal dimension d_f.[32] The fractal dimension represents the agglomerate structure, where a larger d_f indicates a higher level of agglomeration. As listed in the table, the d_f values for the AEI (3.58; 3.56; 3.66) are at least 70% larger than the one obtained for Nafion (2.09). These values suggest that the AEI inks contain larger agglomerates than the ink

based on Nafion. Larger aggregates are suspected to reduce the triple-phase-boundary and catalyst utilization, and therefore lead to poorer performance in the kinetic region.[33] Electrochemical impedance spectroscopy (EIS) recorded at 0.85 V in oxygen at 1600 rpm shows larger diameter semi-circles at low frequencies for the AEIs compared to Nafion (Figure S2). An increased diameter of the low-frequency semi-circle is indicative for increased mass-transfer inhibition of oxygen from the bulk of the solution to the active sites.[34] Therefore, the EIS supports the assumption that the commercial AEIs have slower oxygen-diffusivities. The origin of lower local oxygen transport for the commercial AEIs is suspected to be found in the lack of oxygenophilic perfluorocarbons, which are present in Nafion. Supporting this conclusion, it has been shown that modifying the molecular structure of an AEI, by replacing methyl ($-CH_3$) or trifluoromethyl groups ($-CF_3$) increases the RDE limiting current density by 15% (from 4.5 to 5.3 mA/cm^2).[35]

2.2. Preparation of the catalyst layer for Gas-Diffusion-Electrode (GDE) testing – from ink to morphology

Inks for GDE testing are prepared with a lower ionomer to catalyst ratio (20wt% / 80wt% I/C) compared to RDE inks, (33wt% / 66wt% I/C) following the best reported performance of Fe-N-C Pajarito Powder in AEMFC with ETFE-based radiation-grafted benzyltrimethylammonium-type ionomer.[13] The GDE inks are characterized with rheology and dynamic light scattering (DLS) to gain insights of how the ink microstructure affects the catalyst layer structure. There are a lot of parameters to adjust in the ink composition including types of solvents[36], solvent ratio[37], concentration of catalyst and concentration of ionomer.[38] For the sake of focus on the AEI properties, all these parameters are kept constant and only the type of AEI is changed. Ethanol is chosen as the solvent for the GDE ink as the technical data sheets of all AEIs state solubility in

ethanol[39] or the AEI is supplied in ethanol dispersion, as it is the case for Piperion and Sustainion. In contrast to the RDE inks studied in the previous section, which can be ultrasonicated to re-disperse the ink fully before drop-casting it, the dispersibility of a given catalyst in an ink is crucial in the case of a GDE. The duration of the spraying of the electrode compared to RDE dropcasting is much longer, and precipitation of the ionomer or catalyst in the ink container of the spray gun should be avoided. The concentration of the catalyst in the ink is chosen to be 2 mg_{Cat}/mL (0.2 wt%), as higher concentrations caused frequent clogging of the spray gun needle.

The GDE inks are characterized in a rheology study (Figure 2. a)). The shear stress is linearly increasing with a constant slope for ethanol, slightly deviating from this linear increase at shear rates below 10 s^{-1} for the inks containing the AEIs and Pajarito Powder and the reference with Pajarito Powder in ethanol. The straight line observed for ethanol is typical for Newtonian fluids such as ethanol. The presence of Pajarito Powder with and without AEIs in the inks cause weak shear thickening as can be seen from the minor increase of the shear stress at shear rates below 10 s^{-1}. The viscosity stays constant in the shear rate window from 10 to 100 s^{-1} for all inks (Figure 2. b)). At lower and higher shear rates, the viscosity tends to increase. It can be concluded that the type of AEI does not affect the viscosity of the ink. The aggregates size in the catalyst inks are determined by dynamic light scattering (DLS). The average aggregate sizes for the inks with Pajarito Powder and, Fumion and Piperion AEIs, are distributed between 300 and 700 nm (Figure 2. c)). Most aggregates for these two inks can be found between 400 and 500 nm. A shift of the aggregate distribution by 100 nm to larger aggregates is observed for the ink containing Pajarito Powder and Sustainion AEI.

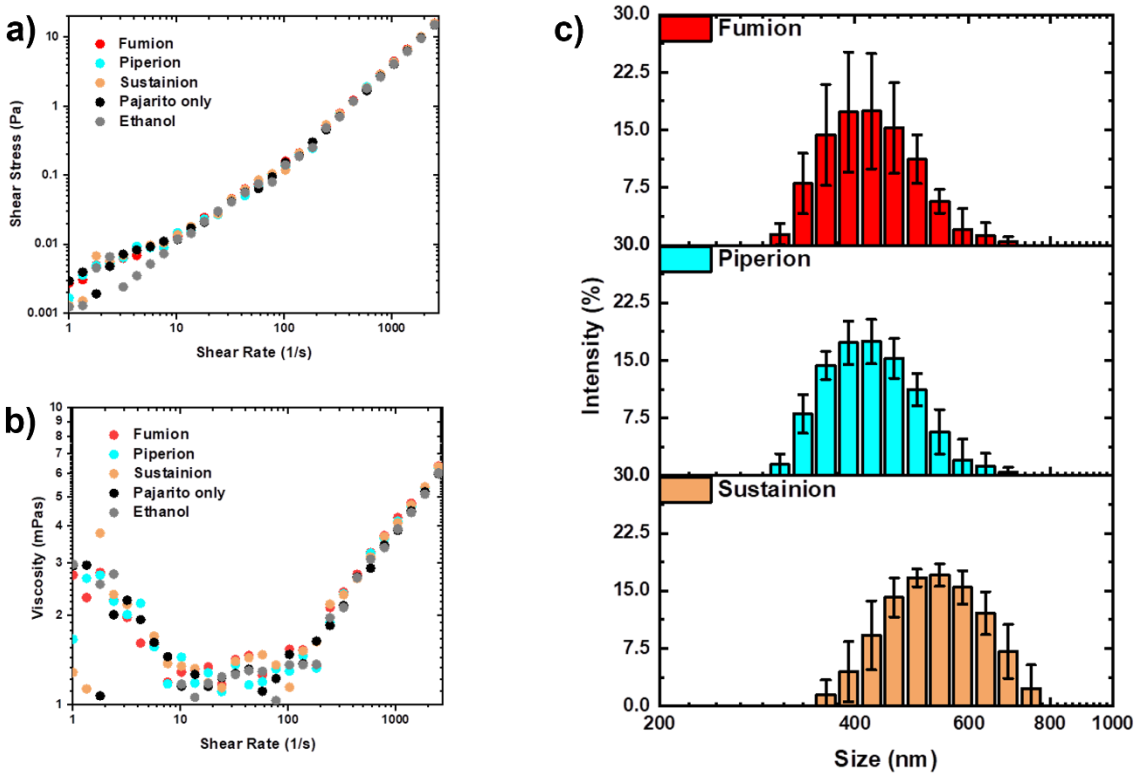

Figure 2. a) Shear stress and b) Viscosity for the AEI/Fe-N-C GDE inks and Fe-N-C only and solvent Ethanol only. c) Aggregate size distribution of the GDE inks.

After spraycoating onto the hydrophobic side of gas-diffusion-layer H23C8 (Freudenberg), the morphologies of the catalyst layers are studied via scanning electron microscopy (SEM) (Figure 3.). The loading of the catalyst layers is verified with cross section imaging. The catalyst loadings have been confirmed by weighing for Fumion AEI as 1.31 $mg_{Fe\text{-}N\text{-}C}$, Piperion AEI as 1.20 $mg_{Fe\text{-}N\text{-}C}$ and Sustainion AEI as 1.28 $mg_{Fe\text{-}N\text{-}C}$. Cross-section images allowed to determine the thicknesses of the films: 40 µm for Fumion AEI/Fe-N-C, 35 µm for Piperion AEI/Fe-N-C, and 40 µm for Sustainion AEI/Fe-N-C. The catalyst layers are showing different surface features. The surface based on Fumion AEI is smooth with catalyst particles forming flat and dense island aggregate structures. In the Piperion AEI-containing catalyst layer, a rough surface with rather

loose out-of-the-surface plane aggregates can be observed, while in the case of the Sustainion AEI based catalyst layer a homogeneous distribution of catalyst particles is observed.

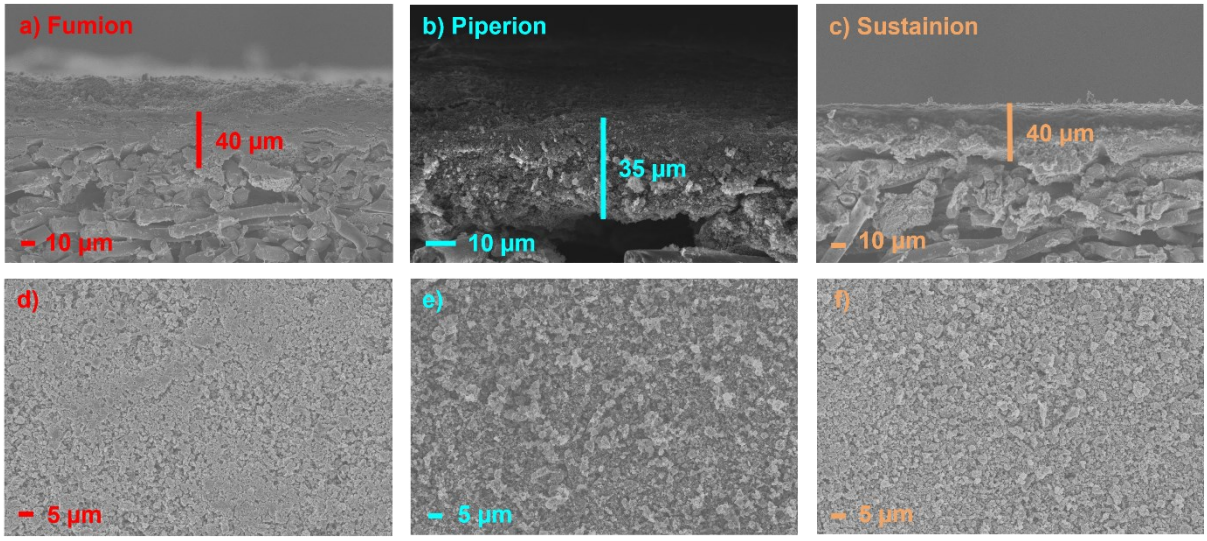

Figure 3. Cross section catalyst layers based of Pajarito Powder and a) Fumion (Loading: 1.31 mg/cm^2), b) Piperion (Loading: 1.20 mg/cm^2) and c) Sustainion (Loading: 1.28 mg/cm^2) and the topviews of catalyst layers with d) Fumion e), Piperion and f) Sustainion before electrochemical characterization.

2.3. Effect of the AEI type on the oxygen reduction reaction performance of Fe-N-C catalyst in alkaline gas-diffusion-electrode

The first analysis of the AEIs combined with membrane in the oxygen reduction reaction (ORR) focuses on the type of ionomer. At high current densities (2 A/cm^2), the average combinations with Piperion AEI have a lower overpotential regardless of the membrane (Figure 4. a)). One potential explanation might be that the Pajarito Powder retains a high BET surface area of 603 m^2/g after integration into the catalyst layer with Piperion AEI compared to the original BET surface area of Pajarito Powder itself (675 m^2/g) (Figure 5. d)). Therefore, there might be more active sites still

accessible at higher current densities. The best performance at high current densities is not achieved by a pair of the same anion conducting polyelectrolyte family, but by Piperion AEI with Sustainion AEM in agreement with the report by Young Moo Lee et al where it was outlined that using the same anion conducting polyelectrolyte as membrane and ionomer might not be the ideal solution due to different requirements for membrane and ionomer.[16] As Sustainion AEM was the membrane, which gave the best combination at high current densities, a combination of unmodified Nafion™ ionomer with Pajarito Powder and Sustainion AEM was also measured (Figure S5). Despite Nafion™ molecular structure is designed for proton transport, it showed a comparable performance to Fumion AEI. Nafion™ has been also used as a binder in an AEMFC, thus, it can be suspected that the water channels might be responsible for the hydroxide transport in the catalyst layer at the high relative humidity.[40] The worst performance at high current densities on average is the combination of Fumion AEI and Fumasep AEM. Among 5 measurements, 4 showed bubble formation in the upper cell compartment opening above the membrane potentially as a result of damage to the membrane at high current densities. For reasons of transparency, it is noted that the curves show slightly lower overpotentials for some samples including Sustainion AEI / Sustainion AEM, Sustainion AEI / Piperion AEM, Piperion AEI / Sustainion AEM at high current densities (1, 1.5 and 2.0 A/cm^2) deviating from the slope, which are time-dependent artefacts. The recorded data is a mixture of time and potential-dependent processes.

Even though the Fumion AEI might not be the most suitable choice at high current densities, Fumion AEI in combination with Piperion AEM demonstrated repeatedly superior performances at lower current densities between 50 and 250 mA/cm^2 (Figure 4. b)). Except for Piperion AEI / Sustainion AEM, Fumion AEI is the preferential choice for low current density operation.

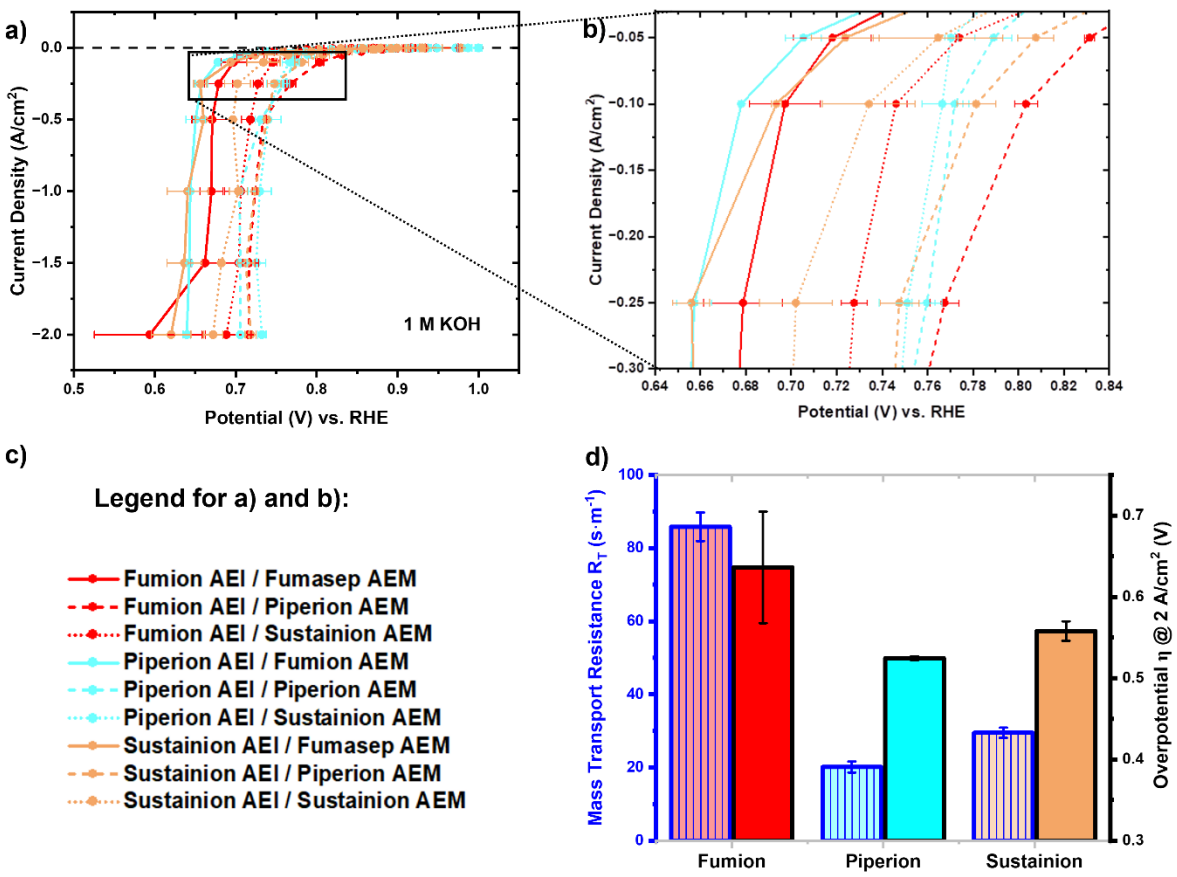

Figure 4. a) Oxygen reduction reaction measurement with GEIS protocol with data plotted to emphasize the effect of the ionomer. The data is recorded in a cell, in which the RHE (RE) is in a separate compartment and a the membrane separates the tested sample (WE) from platinum rod (CE). The GEIS protocol starts with galvanostatic steps and holding time from small current densities to high current densities in the order of - 0.1 mA/cm^2 (90 s), - 1/-2.5/-5/-10 mA/cm^2 (30 s), - 25/-50/-10/-250 mA/cm^2 (5 s), - 0.5/-1.0/-1.5/-2.0 A/cm^2 (5 s) at an oxygen flow rate of 300 mL/min. The last recorded potential value at each galvanostatic step is taken. Each single potential value is iR-compensated with the value of the uncompensated resistance corresponding to the magnitude of the impedance measured after the corresponding galvanostatic step. Thereby, the single frequency for which the phase angle is closest to 0 in the high frequency region > 1000 Hz

is taken. At least two sets of independent GEIS measurements for each type of sample are carried out. It is noted that some curves show slightly lower overpotentials for some samples at high current densities (1, 1.5 and 2.0 A/cm^2) deviating from the curve slope, which are time-dependent artefacts. The recorded data is a mixture of time and potential-dependent processes (Sustainion AEI / Sustainion AEM, Sustainion AEI / Piperion AEM, Piperion AEI / Sustainion AEM). b) Zoom in at lower current density range. c) Legend for plot a) and b). d) Mass Transport Resistance R_T of the catalyst layers with different ionomers at 2.5% O_2 (blue border) besides the potential at 2 A/cm^2 at 100% O_2 (black border). The limiting current i_{lim} for the calculation of the Mass Transport Resistance R_T is determined by stepping the galvanostatic steps intervals of 20 mA/cm^2 with 5 seconds hold time. The limiting current is determined as the last value of current at the potential jump associated with all oxygen being reacted with limiting current data extraction as indicated SI Figure S6. $R_T = \frac{4\,F\,x_0^{dry-in}}{i_{lim}} \frac{p-p_w}{RT}$ with the Faraday constant F = 96485 C/mol, the concentration of O_2 regulated to the dry mole fraction x_0^{dry-in}, p denotes total gas pressure which is atm in the small GDE setup, p_w is the water vapor pressure, T is the absolute cell temperature and R is the universal gas constant. Two independent measurement of a type of sample are used to determine the limiting current.

The superior performance of Piperion AEI at high current density can be further rationalized by the exceptional porosity retention in the catalyst layer. In fact, the BET surface area of Pajarito Powder catalyst decreases by half in the Sustanion AEI and Fumion AEI derived catalyst layers. On the contrary, Piperion AEI offers much higher retention of pores, particularly below 4 nm (Figure 5.).

2.4. The effect of AEI on O_2 mass-transport in the catalyst layer

Due to the thickness of the Fe-N-C based cathodes employed in this study (~40µm for 1.2 $mg_{Fe\text{-}N\text{-}C}$) compared to Pt/C (~ 10 µm)[36], O_2 transport limitations are much more likely in Fe-N-C cathodes. As already observed during ORR measurements in the RDE setup, the diffusion limiting currents in thin film electrodes with AEIs are lower compared to Nafion™ implying a poor O_2 permeability of the AEIs. Despite the reduction of the weight fraction of AEI in the catalyst layers for the GDE studies to reduce the effect of excessive ionomer blockage on oxygen diffusion, gas-phase-transport might be still impeded to a different degree depending on the AEI in the catalyst layer. Limiting current measurement enable to explore the effect of the AEI on the oxygen transport capabilities of the catalyst layer. For the sake of simplicity, the AEI is combined with their respective brand membrane (Fumion AEI/Fumasep AEM, Piperion AEI/Piperion AEM, Sustainion AEI/Sustainion AEM) in the set of experiments for the evaluation of the O_2 mass transport. Limiting current measurements is a widely applied technique to determine the oxygen transport resistance in MEAs in PEMFC.[41,42,43] Nevertheless, the study of oxygen transport in AEMFC remains less explored. Only recently, a protocol was developed to study the O_2 mass transport in GDE setups.[44] Increasing the ionomer to catalyst ratio for Nafion and Pt/C based catalyst layers in acidic environment led to voltages losses at high current densities for high ionomer to catalyst ratio due to oxygen transport limitations. Fumion AEI based catalyst layer has the highest mass transport resistance, followed by Sustainion AEI based catalyst layers. (Figure 4. d)) The lowest mass-transport resistance is measured for the Piperion AEI based catalyst layer. Mass-transfer losses are expected become dominant at high current in the GDE ORR measurement. Therefore, the overpotentials at 2 A/cm^2 are correlated to the mass transport resistance values. The overpotentials at high current densities measured with a concentration of 100% O_2 in GDE follow the same trend

as the R_T values (Figure 4. d)). It can be concluded that the type of ionomer is impacting the oxygen transport in the catalyst layer and thus, the performance at current densities with high oxygen consumption.

2.5. Effect of the AEI on the water vapor sorption capabilities of Fe-N-C catalyst layers

As water is reactant at the cathode in an AEMFC, cathodes are inclined to dry out at high current densities, and therefore, insights into water sorption behavior of the catalyst layers and the interaction of water with the ionomer and pore structure are important to optimize the performance. The water sorption isotherms of all AEIs normalized to the catalyst mass in the respective catalyst layer can be assigned to type 3 isotherms with little sorption at low relative humidity and an exponential sorption at high relative humidity range (Figure 5. c)). Type 3 isotherms indicate that strong adsorbate-adsorbate interactions of water molecules in the vapor dominate over weak adsorbate-adsorbent interactions of water with the hydrophobic properties of catalyst and ionomer.[45] Below 40% relative humidity, the adsorption is controlled by hydrophilic functional groups in the catalyst layer.[46] Therefore, the water uptake at low relative humidity can provide information regarding the hydrophobicity of the ionomers, which decreases in the order of Fumion, Piperion, Sustainion.

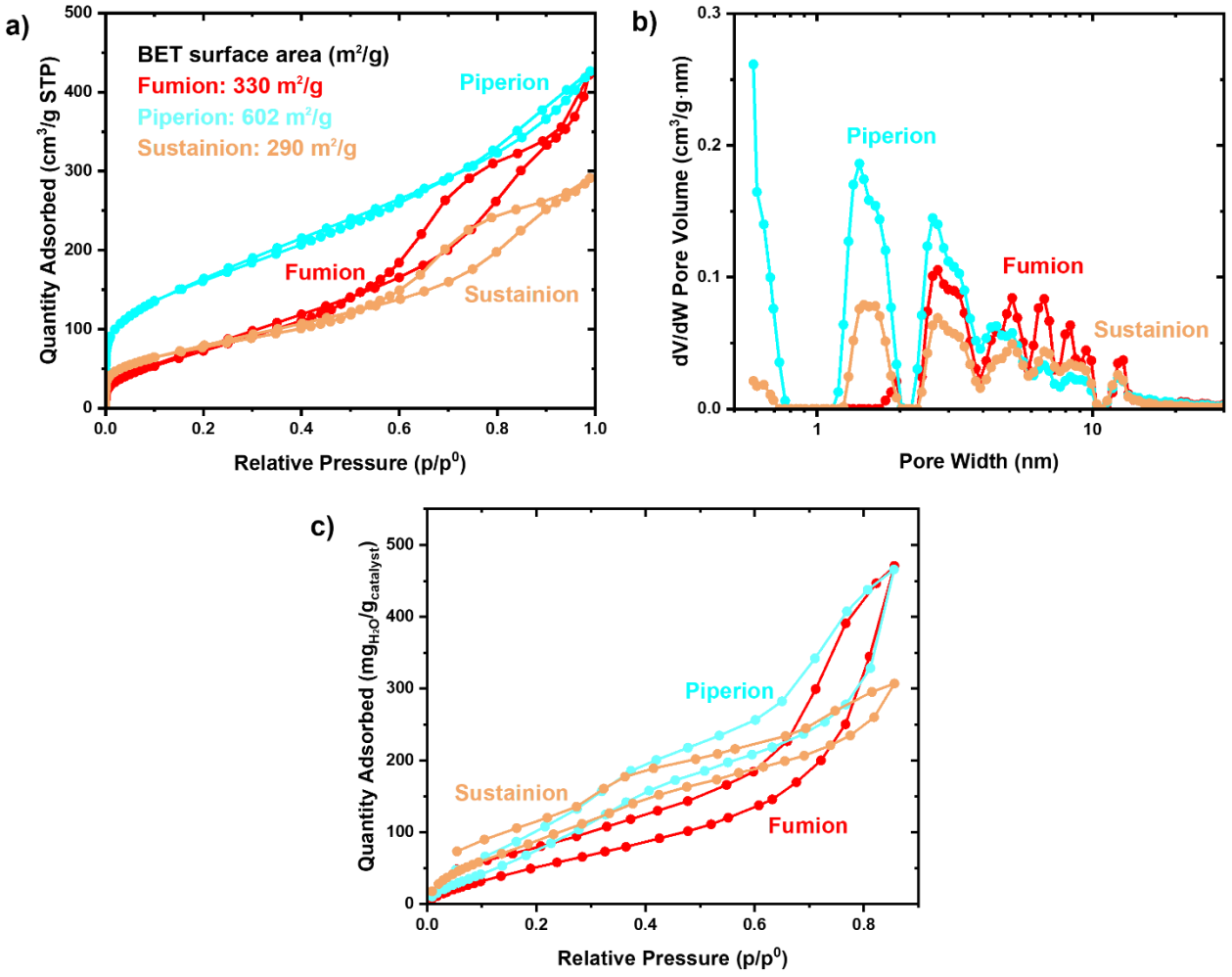

Figure 5. a) Nitrogen sorption isotherm of the catalyst layers sprayed on aluminum foil b) Pore size distribution c) Water Sorption Isotherms before electrochemical characterization.

In the intermediate range of relative humidity, (30% to 80% relative humidity), water molecules form multilayers around hydrophilic sites due to hydrogen bonding and, when these localized clusters of water are saturated, they coalesce, which leads to water clusters and causes capillary condensations.[47] The lower the relative pressure at which the rise begins, the smaller the capillaries, as the onset of condensation shifts to higher pressure with increasing pore size. The

upturn of water adsorption for Piperion AEI at lower relative pressure compared to Fumion AEI is in agreement with the pore size distribution from N_2 sorption data (Figure 5. b)), in which Piperion AEI catalyst layer has more mesopores with 3 nm pore width compared to Fumion AEI based catalyst layer.[48] A steep isotherm at relative humidities higher than 80% implies that secondary pores are filled with water[49], which is pronounced for Fumion AEI catalyst layer with highest mesopore proportion between 5 and 10 nm. Due to the water occupation of secondary pores in Fumion and Piperion AEI catalyst layers, these catalyst layers face higher risk of blocked gas transport at high relative humidity. The similar hysteresis for all AEI/CLs points towards similar water retention capacities. After reducing the relative humidity in the backward scan, Sustainion retains the highest amount of water compared to the other AEIs. The water adsorption isotherm of a catalyst layer with Pajarito Powder and QAPF-4 ionomer (wt%/wt% 0.43 I/C) has been reported with a similar type 3 isotherm.[50] The water adsorption capacity of ~470 mg_{H2O}/g_{cat} (QAPF-4/Catalyst layer) compares to 471 mg_{H2O}/g_{cat} (Fumion AEI/Catalyst layer), 466 mg_{H2O}/g_{cat} (Piperion AEI/Catalyst layer) and 307 mg_{H2O}/g_{cat} (Sustainion AEI/Catalyst layer).

2.6. Effect of the alkaline exchange membrane on the ORR overpotential in the GDE

To obtain a fair comparison between the different AEMs, membranes with similar thicknesses (between 40 and 55 µm) were chosen. At low and high current densities of the ORR, stark differences of 150 mV in overpotential are observed. The potentials are ranging from 0.40 V to 0.53 V at a current density of -0.05 A/cm^2 and from 0.535 V to 0.737 V at -2 A/cm^2. By grouping the AEIs tested according to the membrane, it becomes evident that AEIs tested with Fumasep AEM in general display a higher overpotential (Figure 6. a)). It can also be observed that, while all the electrodes tested with Piperion AEM offered similar performances, the choice of ionomer

had a significant effect on the system based on Sustainion and Fumasep membranes.

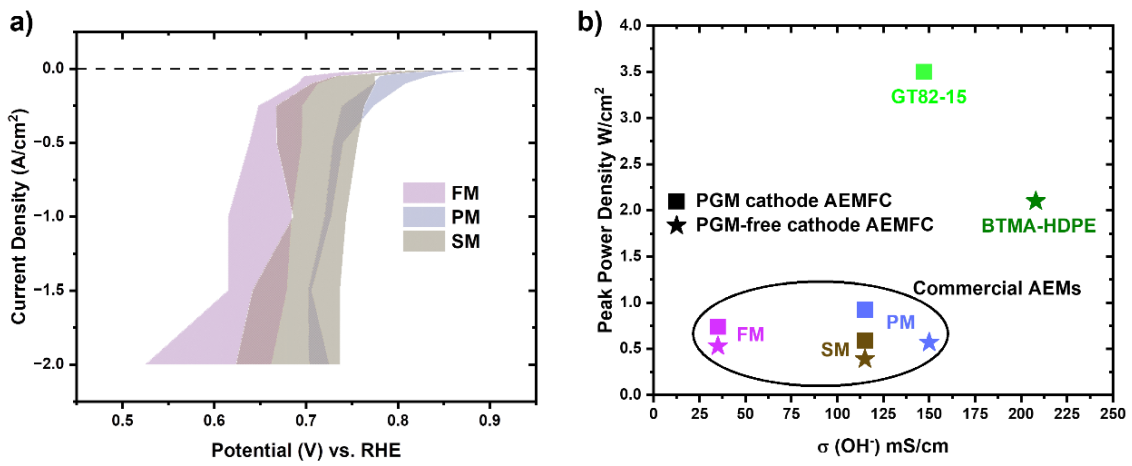

Figure 6. a) The effect of the choice of the AEM membrane. The potential range comprises the values for all AEIs (Fumion AEI, Piperion AEI, Sustainion AEI) tested for that the specific AEM. The GEIS protocol starts with galvanostatic steps and holding time from small current densities to high current densities in the order of - 0.1 mA/cm^2 (90 s), - 1/-2.5/-5/-10 mA/cm^2 (30 s), - 25/-50/-10/-250 mA/cm^2 (5 s), - 0.5/-1.0/-1.5/-2.0 A/cm^2 (5 s) at an oxygen flow rate of 300 mL/min. The last recorded potential value at each galvanostatic step is taken. Each single potential value is iR-compensated with the value of the uncompensated resistance corresponding to the magnitude of the impedance measured after the corresponding galvanostatic step. Thereby, the single frequency for which the phase angle is closest to 0 in the high frequency region > 1000 Hz is taken. At least two sets of independent GEIS measurements for each type of sample are carried out. b) Peak power densities versus hydroxide conductivities of commercial AEMs and best performing AEMs in best reported AEMFCs with PGM- (square) and PGM-free- (star) based cathodes.[6,13,51,52,53,54,55,56,57](Testing conditions and references are listed in Table S5.).

To explain the differences in ORR between the membranes, the hydroxide conductivities (σ(OH$^-$))

of the respective membranes were analyzed. The σ(OH^-) of Fumasep AEM at 25°C, the temperature employed in this study, has been reported to be 21 mS/cm at 25°C, considerably lower than measured at temperatures relevant for AEMFC.[58] On the contrary, the σ(OH^-) of Sustainion AEM and Piperion AEM are reported to be 64 mS/cm at room temperature and 66 mS/cm at 25°C[59], respectively. This trend of hydroxide conductivities correlates to the performance ranges of the respective AEMs in GDE ORR measurements. Other factors beyond the membrane properties could impact the interfacial resistance including the adhesion of catalyst layer to the membrane,[60] or the water transport at the interface between catalyst layer and AEM.[50] Therefore, to put the GDE studies in context with AEMFCs results, the commercial membranes at higher temperature in AEMFCs do not fall into the high performance class of the research lab produced AEMs for both PGM- and PGM-free cathode catalysts (Figure 6. b), Table S5).

3. Conclusions

The RDE screening of catalysts in alkaline medium is recommended to be extended beyond Nafion, to involve AEIs, which are integrating the Fe-N-C catalyst into the MEA cathode. As reduced oxygen permeability has been observed for all AEI in comparison with Nafion, future developments for new AEIs might shift away from using a molecular structure that fulfil the requirements for AEM towards a more AEI-functional design with regard to high oxygen flux and permeability.[35,61] The oxygen diffusion limiting current in RDE is an easy accessible value to check the oxygen transport in new developed AEIs. The RDE studies could be extended to quantify the mass-transport by parameters such as diffusion coefficient and solubility of O_2 in the AEI.[62] Due to reduced components compared to MEA, GDE half cells enable a testing platform to focus on the characterization of a single catalyst layer with application-relevant loading and gas supply.

Blending AEIs with catalyst affect the mesopore and micropore structure of the catalyst material, with Fumion AEI and Sustainion AEI blocking the accessibility of micropores. While the lack of micropores might not be relevant at low current densities in the case of Fumion AEI, at high current densities the Piperion AEI based catalyst layer with the highest BET surface area shows the best performance. Despite similar amounts of water present as a reactant in the Fumion AEI and Piperion AEI catalyst layers at 100% RH, the restricted oxygen transport capabilities limit the performance at high current densities for Fumion AEI. The hydration of the catalyst layer can be further optimized by tailoring the hydrophilic / hydrophobic properties via the polymer chemistry of the AEI.[63] This study confirmed that the membrane's hydroxide conductivity correlates with the performance of the AEM/AEI combination. As the chosen I/C ratio might not be the optimal for each of the AEIs investigated, future work can focus on optimizing the I/C ratio[64,65] in the catalyst layer for an individual AEI and also take the solvent composition[22,22] into account for the adjustment of the pore network of the catalyst layer. Ongoing developments in half-cell setups will enable to study temperature[66] and relative humidity effects on the cathode catalyst layer performance.

Author Contributions

The first draft was written by S.K. and the final manuscript was written through contributions of all authors. S.K. performed the electrochemical measurements, SEM imaging, DLS and viscosity measurements. S. K. conceived the figures, processed and plotted the data. Z. L. helped in the ink preparation, sprayed the catalyst layers for the sorption measurements, and contributed to the GDE measurements. F. A. recorded the USACS/SAXS data of the inks at NCD-SWEET beamline at

ALBA Synchrotron with the collaboration of ALBA staff. A. P. spay coated the GDE samples. S. F. provided the data for the nitrogen and water sorption measurements.

Funding Sources

S. K. is grateful for the financial support via the departmental scholarship. F. A. experiments were funded by the Horizon Europe (HORIZON-INFRA-2021-SERV-01, grant number 101058413) co-funded by UKRI (grand number 10039728) and SERI (contract number 22.00187). A. P. thanks the EPRSC Centre for Doctoral Training in the Advanced Characterisation of Materials (grant number EP/L015277/1). J. B. acknowledges the Imperial College Research Fellowship. S. F. acknowledges funding from the VALUE programme grant (grant number EP/W031019/1). M. T. acknowledges the Royal Academy of Engineering grant. (grand number CiET1819\2\60).

ACKNOWLEDGMENT

S. K. acknowledges the insightful discussions with G. K. H. Wiberg and M. Arenz for the implementation of the GDE half-cell.

References

1. Grot, W. CF=CFCF 2 CF SO F AND DERVATIVES AND POLYMERS THEREOF, **1968**, Patent US3718627A

2. Lim, X. Could the world go PFAS-free? Proposal to ban 'forever chemicals' fuels debate. *Nature* **2023**, 620, 24-27

3. Thompson, S. T.; Peterson, D.; Ho, D.; Papageorgopoulos, D. Perspective-The Next Decade of AEMFCs: Near Term Targets to Accelerate Applied R&D. *J. Electrochem. Soc.* **2020**, 167, 084514

4. Hyun, J.; Kim, H.-T. Powering the hydrogen future: current status and challenges of anion exchange membrane fuel cells. *Energy Environ. Sci.* **2023**, 16, 5633-5662

5. Huang, G.; Mandal, M.; Peng, X.; Yang-Neyerlin, A. C.; Pivovar, B. S.; Mustain, W. E.; Kohl, P. A. Composite Poly(norbornene) Anion Conducting Membranes for Achieving Durability, Water Management and High Power (3.4 W/cm2) in Hydrogen/Oxygen Alkaline Fuel Cells. *J. Electrochem. Soc.* **2019**, 166, F637

6. Mandal, M.; Huang, G.; Ul Hassan, N.; Peng, X.; Gu, T.; Brooks-Starks, A. H.; Bahar, B.; Mustain, W. E.; Kohl, P. A. The Importance of Water Transport in High Conductivity and High-Power Alkaline Fuel Cells. *J. Electrochem. Soc.* **2020**, 167, 054501

7. Ul Hassan, N.; Mandal, M.; Huang, G.; Firouzjaie, H. A.; Kohl, P. A.; Mustain, W. E. Achieving High-Performance and 2000 h Stability in Anion Exchange Membrane Fuel Cells by Manipulating Ionomer Properties and Electrode Optimization. *Adv. Energy Mater.* **2020**, 10, 2001986

8. Hossen, M. M.; Hasan, M. S.; Sardar, M. R. I.; bin Haider, J.; Mottakin; Tommeveski, K.; Atanassov, P. State-of-the-art and developmental trends in platinum group metal-free cathode catalyst for anion exchange membrane fuel cell (AEMFC). *Appl. Cat. B: Environ.* **2023**, 325, 121733

9. Firouzjaie, H. A.; Mustain, W. E. Catalytic Advantages, Challenges, and Priorities in Alkaline Membrane Fuel Cells. *ACS Catal.* **2020**, 10 (1), 225-234

10. Ramaswamy, N.; Mukerjee, S. Fundamental Mechanistic Understanding of Electrocatalysis of Oxygen Reduction on Pt and Non-Pt Surfaces: Acid versus Alkaline Media. *Adv. Phys. Chem.* **2012**, 491604

11. García, A.; Pascual, L.; Ferrer, P.; Gianolio, D.; Held, G.; Grinter, D. C.; Peña, M. A.; Retuerto,

M.; Rojas, S.. Study of the evolution of FeN_xC_y and Fe_3C species in Fe/N/C catalysts during the oxygen reduction reaction in acid and alkaline electrolyte. *J. Power Sources* **2021**, 490, 229487

12. Mehmood, A.; Ali, B.; Gong, M.; Kim, M. G.; Kim, J.-Y.; Bae, J.-W.; Kucernak, A.; Kang, Y.-M.; Nam, K.-W.. Development of a highly active Fe-N-C catalyst with the preferential formation of atomic iron sites for oxygen reduction in alkaline and acidic electrolytes. *J. Colloid Interface Sci.* **2021**, 596, 148-157

13. Adabi, H., Shakouri, A.; Ul Hassan, N.; Varcoe, J. R.; Zulevi, B.; Serov, A.; Regalbuto, J. R.; Mustain, W. E.. High-performance commercial Fe-N-C cathode electrocatalyst for anion-exchange membrane fuel cells. *Nat. Energy* **2021**, 6, 834-843

14. Firouzjaie, H. A.; Mustain, W. E. Catalytic Advantages, Challenges, and Priorities in Alkaline Membrane Fuel Cells. *ACS Catal.* **2020**, 10 (1), 225-234

15. Adabi, H.; Santori, P. G.; Shakouri, A.; Peng, X.; Yassin, K.; Rasin, I. G.; Brandon, S.; Dekel, D. R.; Ul Hassan, N.; Sougrati, M.-T.; Zitolo, A.; Varcoe, J. R.; Regalbuto, J. R.; Jaouen, F.; Mustain, W. E. Understanding how single-atom site density drives the performance and durability of PGM-free Fe-N-C cathodes in anion exchange membrane fuel cells. *Mater. Today Adv.* **2021**, 12, 100179

16. Chen, N.; Lee, Y. M. Anion exchange polyelectrolytes for membranes and ionomers. *Prog. Polym.* **2021**, 113, 101345

17. Yang, Y.; Li, P.; Zheng, X.; Sun, W.; Dou, S. X.; Ma, T.; Pan, H. Anion-exchange membrane water electrolyzers and fuel cells. *Chem. Soc. Rev.* **2022**, 51, 9620-9693

18. Wang, J.; Zhao, Y.; Setzler, B. P.; Rojas-Carbonell, S.; Yehuda, C. B.; Amel, A.; Page, M.; Wang, L.; Hu, K.; Shi, L.; Gottesfeld, S.; Xu, B.; Yan, Y. Poly(aryl piperidnium) membranes and

ionomers for hydroxide exchange membrane fuel cells. *Nat. Energy* **2019**, 4, 392-398

19. Favero, S.; Stephens, I. E. L.; Titirici, M.-M.. Anion Exchange Ionomers: Design Considerations and Recent Advances-An Electrochemical Perspective. *Adv. Mater.* **2023**, 36, 2308238

20. Song, W.; Zhang, X.; Yang, C.; Yang, Z.; Wu, L.; Ge, X.; Xu, T. Alkaline Membranes toward Electrochemical Energy Devices: Recent Development and Future Perspectives. *ACS Cent. Sci.* **2023**, 9 (8), 1538-1557

21. Ehelebe, K; Schmitt, N.; Sievers, G.; Jensen, A. W.; Hrnjić, A.; Jiménez, P. C.; Kaiser, P.; Geuß, M.; Ku, Y.-P.; Jovanovič, P.; Mayrhofer, K. J. J.; Etzold, B.; Hodnik, N.; Escudero-Escribano, M.; Arenz. M.; Cherevko, S. Benchmarking Fuel Cell Electrocatalysts Using Gas Diffusion Electrodes: Inter-lab Comparison and Best Practices. *ACS Energy Lett.* **2022**, 7 (2) , 816-826

22. Han, C.; Shi, W.; Huang, M.; Wang, Q.; Yang, J.; Chen, J.; Ding, R.; Yin, X. Solvent Effect on the Catalyst Ink and Layer Microstructure for Anion Exchange Membrane Fuel Cells. *ACS Appl. Mater. Interfaces* **2024**, 16 (4), 4550-4560

23. Ehelebe, K.; Ashraf, T.; Hager, S.; D. Seeberger, D.; Thiele, S.; Cherevko, S. Fuel cell catalyst evaluation using a gas diffusion electrode half-cell: Oxygen reduction reaction on Fe-N-C in alkaline media. *Electrochem. Commun.* **2020**, 116, 106761

24. Wiberg, G. K. H.; Nösberger, S.; Arenz, M. Evolution of a GDE setup: Beyond ambient conditions. *Curr. Opin. Electrochem.* **2022**, 36, 101129

25. Mazzoli, L.; Pedersen, A.; Kellner, S.; Hunter, R. D.; Cai, R.; Wang, M.; Sivula, K.; Haigh, S. J.; Barrio, J.. Inducing Porosity in Xylose-derived FeNC Electrocatalysts for Alkaline Oxygen Reduction. *Green Chem.* **2024**, 26, 3271-3280

26. Beltrán, D. E.; Litster, S. Half-Wave Potential or Mass Activity? Characterizing Platinum Group Metal-Free Fuel Cell Catalysts by Rotating Disk Electrodes. *ACS Energy Lett.* **2019**, 4 (5), 1158-1161

27. Hossen, M. M.; Artyushkova, K; Atanassov, P.; Serov, A. Synthesis and characterization of high performing Fe-NC catalyst for oxygen reduction reaction (ORR) in Alkaline Exchange Membrane Fuel Cells. *J. Power Sources* **2018**, 375, 214-221

28. Peng, L.; Yang, J.; Yang, Y.; Qian, F.; Wang, Q.; Sun-Waterhouse, D.; Shang, L.; Zhang, T.; Waterhouse, G. I. N. Mesopore-Rich Fe-N-C Catalyst with FeN4-O-NC Single-Atom Sites Delivers Remarkable Oxygen Reduction Reaction Performance in Alkaline Media, *Adv. Mater.* **2022**, 34, 2202544

29. Santori, P. G.; Mondal, A. N.; Dekel, D. R.; Jaouen, F. The critical importance of ionomers on the electrochemical activity of platinum and platinum-free catalysts for anion-exchange membrane fuel cells. *Sustain. Energy Fuels* **2020**, 4, 3300-3307

30. Daems, N.; Breugelsman, T.; Vankelecom, I. F. J.; Pescarmona, P. P. Influence of the Composition and Preparation of the Rotating Disk Electrode on the Performance of Mesoporous Electrocatalysts in the Alkaline Oxygen Reduction Reaction. *ChemElectroChem* **2018**, 5, 119-128

31. Zhong, G.; Xu, S.; Liu, L.; Zheng, C. Z.; Dou, J.; Wang, F.; Fu, X.; Liao, W.; Wang, H. Effect of Experimental Operations on the Limiting Current Density of Oxygen Reduction Reaction Evaluated by Rotating-Disk Electrode. *ChemElectroChem* **2020**, 7, 1107-1114

32. Osmieri, L.; Wang, G.; Cetinbas, F. C.; Khandavalli, S.; Park, J.; Medina, S.; Mauyer, S. A.; Ulsh, M.; Pylypenko, S.; Myers, D. J.; Neyerlin, K. C. Utilizing ink composition to tune bulk-electrode gas transport, performance, and operational robustness for a Fe-N-C catalyst in polymer

electrolyte fuel cell. *Nano Energy* **2020**, 75, 104943

33. Wang, M; Park, J. H.; Kabir, S.; Neyerlin, K. C.; Karikuki, N. N.; Lv, H.; Stamenkovic, V. R.; Myers, D. J.; Ulsh, M.; Mauger, S. A. Impact of Catalyst Ink Dispersing Methodology on Fuel Cell Performance Using in-Situ X-ray Scattering, *ACS Appl. Energy Mater.* **2019**, 2, 6417-6427

34. Singh, R. K.; Devivaraprasad, R.; Kar, T.; Chakraborty, A.; Neergat, M. Electrochemical Impedance Spectroscopy of Oxygen Reduction Reaction (ORR) in a Rotating Disk Electrode Configuration: Effect of Ionomer Content and Carbon-Support. *J. Electrochem. Soc.* **2015**, 162, F489

35. Yu, W.; Xu, Y.; Shen, X.; Yang, X.; Liu, Z.; Wang, H.; Liang, X.; Ge, X.; Guiver, M. D.; L. Wu, L.; T. Xu, T. Ionomer boosts catalyst layer oxygen transport and membrane conduction for fuel cells. *Next Energy* **2024**, 3, 100104

36. Britton, B.; Holdcroft, S. The Control and Effect of Pore Size Distribution in AEMFC Catalyst Layers. *J. Electrochem. Soc.* **2016**, 163, F353-F358

37. Khandavalli, S.; Iyer, R.; Park, J. H.; Myers, D. J.; Neyerlin, K. C.; Ulsh, M.; Mauger, S. A. Effect of Dispersion Medium Composition and Ionomer Concentration on the Microstructure and Rheology of Fe-N-C Platinum Group Metal-free Catalyst Inks for Polymer Electrolyte Membrane Fuel Cells. *Langmuir* **2020**, 36, 12247-12260

38. Sebastián, D.; Lemes, G.; Luque-Centeno, J. M.; Martínez-Huerta, Pardo, J. I.; Lázaro, M. J. Optimization of the Catalytic Layer for Alkaline Fuel Cells Based on Fumatech Membranes and Ionomer. *Catalysts* **2020**, 10, 1353

39. https://www.bwt.com/en/-/media/bwt/fumatech/datasheets/new/fumion/fumion-faa-3-shredded-film.pdf?rev=35904cd7e67944a38279064513d904ff

40. He, Q.; Zeng, L.; Wang, J.; Jiang, J.; Zhang, L.; Wang, J.; Ding, W.; Wei, Z. Polymer-coating-induced synthesis of FeN_x enriched carbon nanotubes as cathode that exceeds 1.0Wcm^{-2} peak power in both proton and anion exchange membrane fuel cells. *J. Power Sources* **2021**, 489, 229499

41. Beuscher, U. Experimental method to determine the mass transport resistance of a polymer electrolyte fuel cell. *J. Electrochem. Soc.* **2006**, 153 (9), A1788

42. Nonoyama, N.; Okazaki, S.; Weber, A. Z.; Ikogi, Y.; Yoshida, T. Analysis of oxygen-transport diffusion resistance in proton-exchange-membrane fuel cells. *J. Electrochem. Soc.* **2011**, 158 (4), B416

43. Baker, D. R.; Caulk, D. A.; Neyerlin, K. C.; Murphy., M. W. Measurement of oxygen transport resistance in PEM fuel cells by limiting current methods. *J. Electrochem Soc.*, **2009**, 156 (9), B991

44. Lauf, P.; Lloret, V.; Geuß, M.; Collados, C. C.; Thommes, M.; Mayrhofer, K. J. J.; Ehelebe, K.; Cherevko, S. Characterization of Oxygen and Ion Mass Transport Resistance in Fuel Cell Catalyst Layers in Gas Diffusion Electrode Setups. *J. Electrochem. Soc.* 2023, 170 (6), 064509

45. Liu, L.; Tan, S. J.; Horikawa, T.; Do, D. D.; Nicholson, D., Liu, J. Water adsorption on carbon-A review. *Adv. Colloid Interface Sci.* **2017**, 250, 64-78

46. Soboleva, T.; Malek, K.; Xie, Z.; Navessin, T.; Holdcroft, S. PEMFC Catalyst Layers: The Role of Micropores and Mesopores on Water Sorption and Fuel Cell Activity. *ACS Appl. Mater. Interfaces* **2011**, 3 (6), 1827-1837

47. Piece, C.; Smith, N. R.; Wiley, J. W.; Cordes, H. Adsorption of Water by Carbon. *J. Am. Chem Soc.* **1951**, 73, 4551-4557

48. Thommes, M. ; Morell, J. ; Cychosz, K. A. ; Fröba, M. Combining Nitrogen, Argon, and Water

Adsorption for Advanced Characterization of Ordered Mesoporous Carbons (CMKs) and Periodic Mesoporous Organosilicas (PMOs). *Langmuir* **2013**, 29 (48), 14893-14902

49. Mashio, T.; Sato, K.; Ohma, A. Analysis of water adsorption and condensation in catalyst layers for polymer electrolyte fuel cells. *Electrochim. Acta* **2014**, 140, 238-249

50. Otsuji, K.; Shirase, Y.; Asakawa, T.; Yokota, N.; Nagase, K.; Xu, W.; Song, P.; Wang, S.; Tryk, D. A.; Kakinuma, K.; Inukai, J.; Miyatake, K.; Uchida, M. Effect of water management in membrane and cathode catalyst layers on suppressing the performance hysteresis phenomenon in anion-exchange membrane fuel cells. *J. Power Sources* **2022**, 522, 230997

51. Cha, M. S.; Park, J. E.; Kim, S.; Han, S.H.; Shin, S. H.; Yang, S. H.; Kim T. H.; Yu, D. M.; So, S.; Hong, Y. T.; Yoon, S. J.; Oh, S. G.; Kang, S. Y.; Kim, O. H.; Park, H. S.; Bae, B.; Sung, Y. E.; Cho, Y. E.; Lee, J. Y. Poly(carbazaole)-based anion-conducting materials with high performance and durability for energy conversion devices. *Energy Environ. Sci.* **2020**, 13, 3633-3645

52. Zhegur-Khais, A.; Kubannek, F.; Krewer, U.; Dekel, D. R. Measuring the true hydroxide conductivity of anion exchange membranes. *J. Membr. Sc.* **2020**, 612, 118461

53. Kim, M.-J.; Kim, S.; Park, J. E.; Hwang, C.-C.; Lee, S.; Kang, S. Y.; Jung, D.; Cho, Y.-H.; Kim, J.; Lee, K.-S.; Sung, Y.-E. Controlling active sites of Fe-N-C electrocatalysts for oxygen electrocatalysis. *Nano Energy* **2020**, 78, 105395

54. Calderon, J.; Huq, N.; Zheng, M.; Zhou, Y. Power Enhancement of Anion Exchange Membrane Fuel Cells (AEMFCs) Through Spray-Coating of Membrane With Partially Reduced Graphene Oxide. *J. Undergrad. Chem. Eng. Res.* **2022**, 75

55. Liu, Z.; Sajjad, S. D.; Gao, Y.; Yang, H.; Kaczur, J. J.; Masel, R. I. Int. J. Hydrog. Energy, The effect of membrane on an alkaline water electrolyzer. *Int. J. Hydrog. Energy* **2017,** 42, 29661-

29665

56. Raut, A.; Fang, H.; Lin, Y.-C.; Fu, S.; Sprouster, D.; Shimogawa, R.; Frenkel, A. I.; Bae, C.; Douglin, J. C.; Lillojad, J.; Tammeveski, K.; Zeng, Z.; Bliznakov, S.; Rafailovich, M.; Dekel, D. R. Migration and Precipitation of Platinum in Anion-Exchange Membrane Fuel Cells. *Angew. Chem. Int. Ed.* **2023**, 62, e202306754

57. Hyun, J.; Lee, D. W.; Oh, E.; Bae, H.; Park, J.; Doo, G.; Kim, H.-T. Manufacturing and structural control of slurry-cast catalyst layers for AEMFC. *J. Power Sources* **2023**, 573, 233161

58. Cha, M. S.; Park, J. E.; Kim, S.; Han, S.H.; Shin, S. H.; Yang, S. H.; Kim T. H.; Yu, D. M.; So, S.; Hong, Y. T.; Yoon, S. J.; Oh, S. G.; Kang, S. Y.; Kim, O. H.; Park, H. S.; Bae, B.; Sung, Y. E.; Cho, Y. E.; Lee, J. Y. Poly(carbazaole)-based anion-conducting materials with high performance and durability for energy conversion devices. *Energy Environ. Sci.* **2020**, 13, 3633-3645

59. Chae, J. E.; Choi, J.; Lee, S.; Park, C.; Kim, S. Effects of fabrication parameters of membrane-electrode assembly for high-performance anion exchange membrane fuel cells. *J. Ind. Eng. Chem.* **2023**, 133, 255-262

60. Hu, C.; Kang, H. W.; Jung, S. W.; Zhang, X.; Lee, Y. J.; Kang, N. Y.; Park, C. H.; Lee, Y. M. Stabilizing the Catalyst Layer for Durable and High Performance Alkaline Membrane Fuel Cells and Water Electrolyzers. *ACS Cent. Sci.* **2024**, 10 (3), 603-614

61. Yu, W.; Zhang, J.; Huang, D. M.; Liang, X.; Zhang, K.; Xu, Y.; Zhang, H.; Ye, B.; Ge, X.; Xu, T.; Wu, L. Molecular-Level Control over Oxygen Transport and Catalyst-Ionomer Interaction by Designing Cis-Trans Isomeric Ionomers. *ACS Energy Lett.* **2023**, 8 (1), 790-799

62. Khadke, P. S.; Krewer, U. J. Mass-transport characteristics of oxygen at Pt/anion exchange ionomer interface. *Phys. Chem. C* **2014**, 118 (21), 11215-11223

63. Ul Hassan, N.; Mandal, M; Huang, G.; Firouzjaie, H. A.; Kohl, P. A.; Mustain, W. E. Achieving high-performance and 2000 h stability in anion exchange membrane fuel cells by manipulating ionomer properties and electrode optimization. *Adv. Energy. Mater.* **2020**, 10 (40), 2001986

64. Zhou, Y.; Yu, H.; Xie, F.; Zhao, Y.; Sun, X.; Yao, D.; Jiang, G.; Geng, J.; Shao, Z. Improving cell performance for anion exchange membrane fuel cells with FeNC cathode by optimizing ionomer content. *J. Int. Hydrog. Energy* **2023**, 48, 5266-5275

65. Carlson, A.; Shapturenka, P.; Eriksson, B.; Lindbergh, G.; Lagergren, C.; Lindström, R. W. Electrode parameters and operating conditions influencing the performance of anion exchange membrane fuel cells. *Electrochim. Acta* **2018**, 277, 151-160

66. Gridin, V.; Du, J.; Haller, S.; Theis, P.; Hofmann, K.; Wiberg, G. K. H.; Kramm, U. I.; Arenz, M. GDE vs RDE: Impact of operation conditions on intrinsic catalytic parameters of FeNC catalyst for the oxygen reduction reaction. *Electrochim. Acta* **2023**, 444, 142012